Testing the Drop-Size Distribution Based Separation of Stratiform and Convective Rain Using Radar and Disdrometer Data from a Mid-latitude Coastal Region

Merhala Thurai [1,*], Viswanathan Bringi [1], David Wolff [2], David Marks [2,3] and Charanjit Pabla [2,3]

[1] Department of Electrical and Computer Engineering, Colorado State University, Fort Collins, CO 80523, USA; merhala@colostate.edu (M.T.); bringi@engr.colostate.edu (V.N.B.)

[2] NASA GSFC Wallops Flight Facility, Wallops Island, Virginia, USA; david.b.wolff@nasa.gov (D.B.W.), david.a.marks@nasa.gov (D.A.M.); charanjit.s.pabla@nasa.gov (C.S.P.)

[3] Science Systems and Applications, Inc., Lanham, MD, USA; david.a.marks@nasa.gov (D.A.M); charanjit.s.pabla@nasa.gov (C.S.P.)

* Correspondence: merhala@colostate.edu; Tel.: +1-970-491-7678

Abstract: Stratiform and convective rain are associated with different microphysical processes and generally produce drop size distributions (DSDs) with different characteristics. A previous study, using data from a tropical coastal location found that the two rain types could be separated in the N_W–D_m space, where D_m is the mass-weighted mean diameter and N_W is the normalized intercept parameter. The separation method has also been tested using data and observations from a mid-latitude continental location with semi-arid climate, and a sub-tropical continental location. In this paper, we investigate the same separation technique using data and observations from a mid-latitude coastal region. Three-minute DSDs from disdrometer measurements are used for the N_W versus D_m based classification and are compared with simultaneous observations from an S-band polarimetric radar 38 km away from the disdrometer site. Specifically, RHI (range-height indicator) scans over the disdrometer were used for confirmation. Results show that there was no need to modify the separation criteria from previous studies. Scattering calculations using the three-minute DSDs were used to derive retrieval equations for N_w and D_m for the S-band radar and applied to the RHI scans to identify convective and stratiform rain regions. Two events are shown as illustrative examples.

Keywords: stratiform rain; convective rain; raindrop size distributions; polarimetric radar retrievals

1. Introduction

The importance of classification of rain types as convective and stratiform is related to the very different microphysical processes that go into the formation of their respective drop size distributions (DSD). It is well-known (eg., [1]) that stratiform rain is defined by large areas of weak vertical air motion with the dominant feature being the reflectivity bright band where snow aggregates (falling slowly ~ 1 m/s) melt to rain whereas convective rain forms from melting graupel and hail in compact reflectivity "cells" within strong downdrafts. This leads to different methods of estimating rain rates for hydrology as well as calculating the latent heating (vertical) profiles in the stratiform and convective rain areas [2]. Houze [3] has clearly shown the impact of the latent heating profiles on precipitation evolution. Furthermore, while the stratiform rain rates are typically < 10 mm/h, their large areal extent and long duration (e.g., outer rain bands of hurricanes) relative to convective rain make the classification an important topic of study.

Differences in drop size distributions (DSDs) between stratifrom and convective rain have also been examined in the past by several researchers, e.g. [4], [5], and [6], who used ground-based disdrometer data, as well as [7], [8], [9], and [10], who used aircraft data (from particle imaging probes). More recently, Bukovcic et al. [11] used DSD data from a 2D video disdrometer (2DVD: [12], [13]) in central Oklahoma to separate stratiform and convective rain by applying a multi-variable Bayesian classification algorithm whereas Bringi et al. [14] used dual-polarized radar, dual-frequency profilers, and ground-based Joss-Waldvogel disdrometer data to investigate the use of two main parameters governing the DSD characteristics for the separation. Specifically they found that the two rain types could be separated in the $N_W - D_m$ space, where D_m is the mass-weighted mean diameter and N_W is the normalized intercept parameter. The data used in that study (see also [15]) were obtained from Darwin, Australia, which is a tropical oceanic location. Since then, the separation technique has been tested using data and observations from Huntsville, Alabama, USA, [16] a sub-tropical continental location as well as Greeley, Colorado, USA, [17], a mid-latitude continental location with semi-arid climate. For the Huntsville events, 2DVD data were used for the separation method and validation was provided by simultaneous observations from a UHF Doppler profiler collocated with the 2DVD. For the Greeley events, composited DSD data from 2DVD and an optical array probe called the Meteorological Particle Spectrometer (MPS: [18], [19], [20]) were used and validation was provided by RHI (range-height indicator) scans by an S-band polarimetric radar (named CSU-CHILL radar, [21]) over the ground-based instruments.

In this paper, we investigate the same separation technique using data and observations from a mid-latitude coastal region, situated in the Delmarva peninsula in Virginia. As with the Greeley cases, measurements from a 2DVD and an MPS were used to construct the full DSD spectra and the N_W versus D_m based separation is compared with simultaneous observations from an S-band polarimetric radar located 38 km away from the disdrometer site. Three-minute DSDs are used for the classification and RHI radar scans over the disdrometer are used for testing. Three very different rain events are considered.

2. Instrumentation and Observations

2.1. DSD

The instrumentation location belongs to the NASA Wallops Flight Facility (WFF) and is part of the ground validation activities in support of the Global Precipitation Measurement (GPM) Mission [22] as well as studies on precipitation microphysics, e.g. [23]. The ground instruments include many different types of disdrometers and rain gauges including an MPS, several 2DVDs and a Pluvio rain gauge [24], all collocated at the same coastal site. The MPS and one of the 2DVD units is installed within a 2/3rd scaled double wind fence (DFIR; [25]) in order to reduce the effects of high winds on the measurements of small drops. The MPS is used for relatively accurate measurements of drop concentration of small drops (< 1 mm drop diameter), and the 2DVD provided more accurate measurements for the larger diameters, i.e. > 1 mm. The composite or the full DSD is then constructed using the MPS and the 2DVD measurements over–a three-minute time interval. The overlap region has been investigated before [26]; the study found that the best agreement between the two instruments was obtained in the diameter range of 0.75 - 1 mm.

2.2. Radar Observations

The polarimetric radar used for confirmation in this study is the NPOL radar [27] located NNE of the disdrometer site, as shown in Figure 1. The azimuth of the disdrometers (shown in orange) from the radar is 197 deg. The radar scan strategy included volume scans, RHI scans with azimuths of 195, 197 and 199 degrees and, for Z_{dr} calibration, 90 degree elevation 'birdbath' scans. This sequence was repeated regularly, every 7 minutes and 15 seconds. RHI scans along the 197 degree azimuth were chosen for classifying stratiform or convective rain in this study. Specifically, vertical

profiles of reflectivity (Z_h), differential reflectivity (Z_{dr}) and copolar correlation coefficient (ρ_{hv}) were extracted over the disdrometer site to establish whether or not the melting layer can be clearly distinguished well above the ground level.
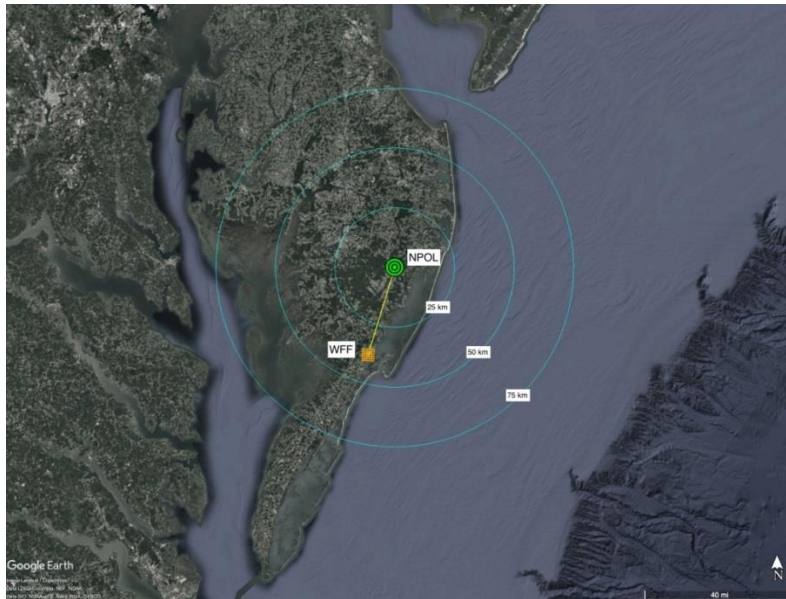

Figure 1. NPOL radar and the disdrometer location.

2.3 Rain events

We consider three events here: (i) a category-1 Hurricane event (Dorian) whose rain-bands passed over the WFF site on 06 September 2019 ([28], [29]); (ii) a squall-line event with a not-so well organized line convection which occurred on 14 October 2019; and (iii) a more widespread event with small embedded convective cells which occurred on 16 October 2019.

For all cases, the NPOL radar had performed the regular routine scans. Figure 2 shows two examples of RHI scans over the disdrometer, one on the 16th of October (Z_h in panel (a) and Z_{dr} in panel (b)) and the other on the 14th of October 2019 (Z_h in panel (c) and Z_{dr} in panel (d)). The top two panels show stratiform rain over the disdrometer site (which is marked with vertical black lines), indicated by the clear presence of radar bright band caused by the melting layer between 3 and 3.5 km height above ground level (a.g.l.). The melting layer is visible in both Z_h and Z_{dr}. By contrast, panels (c) and (d) do not show any radar bright-band in the entire RHI scan, thus it can be classified as convective rain. Panels (e) and (f) show the 1-minute composite DSDs measured by the disdrometers at the same times as panels (a)/(b) and (c)/(d), respectively. For the latter, larger drops can be seen, with maximum recorded diameter (equi-volume drop diameter, D_{eq}) of nearly 4 mm whereas for the former it is just over 3 mm.

Two further examples are given in Fig. 3. Panels (a) and (b) correspond to the Dorian rain-bands event on 6 September 2019, showing very clear bright band between 4 and 4.5 km a.g.l., and panels (c) and (d) show another convective rain example that occurred on 14 October 2019. Once again, the black lines indicate the location of and over the disdrometers. Vertical profiles of Z_h and ρ_{hv} over the disdrometer site for the stratiform rain case (panels (a)/(b)) are shown in panels (e) and (f) and those for the convective rain case (panels (c)/(d)) are shown in panels (g) and (h). In all cases, vertical profiles were extracted over a 37 to 39 km range interval.

Clear differences are seen: (i) the Z_h profile for the stratiform rain in Figure 3 show very clear peak at around 4 km height unlike the convective rain, where the Z_h profiles are 'noisy' and do not show any clearly defined features. (ii) the ρ_{hv} profiles show a 'dip' just below the melting layer in panel (e) for the stratiform rain whereas the convective rain profiles in panel (h) show almost constant ρ_{hv} of 0.99. Such features are used to identify (or classify) the two rain types.
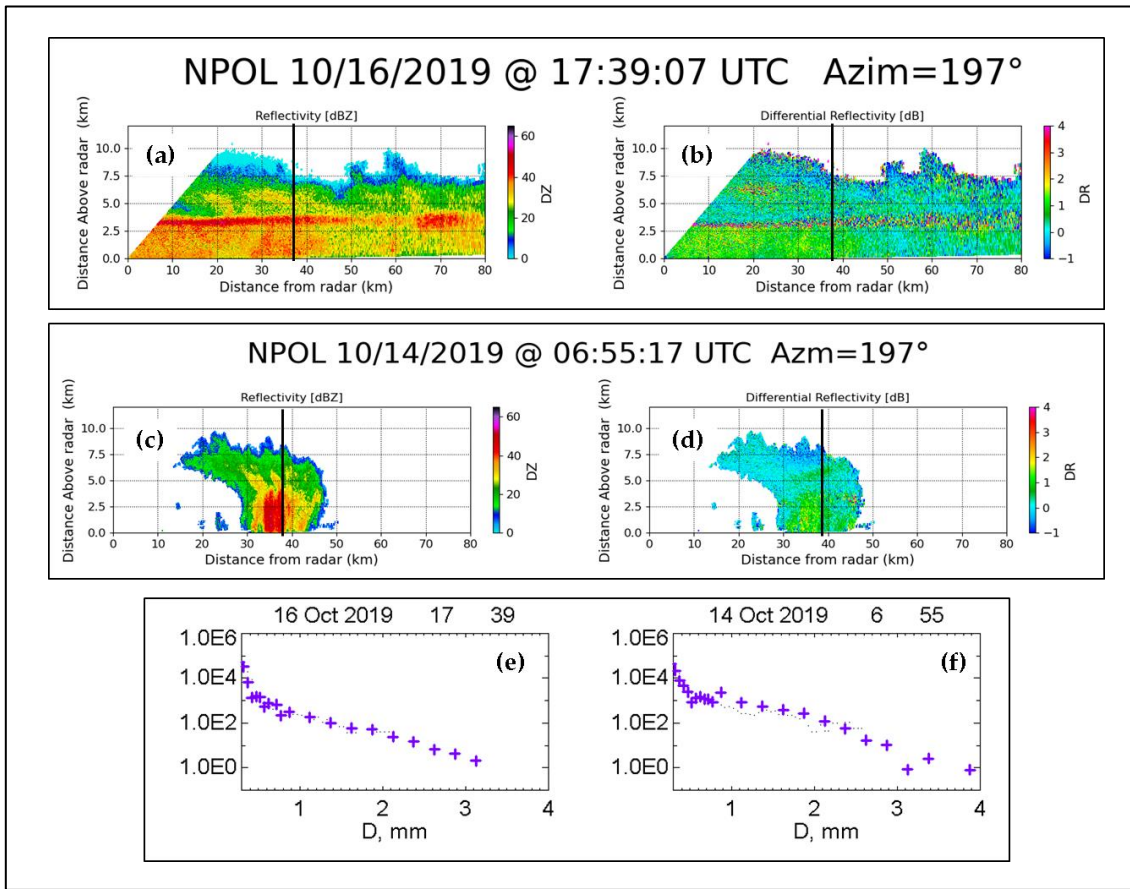
3

Figure 2. (a) RHI scan of Z_h and **(b)** Z_{dr} during a stratiform rain event on 16 October 2019; **(c)** and **(d)** RHI scans of Z_h and Z_{dr} during a convective rain event on 14 October 2019; **(e)** 1-minute composite DSD from disdrometers for case (a); **(f)** 1-minute DSD for case (c). The vertical black lines in the RHI scan correspond to the range of (& height above) the disdrometers.

3. N_w versus D_m variations

1-minute DSDs for the four cases in Fig. 2 and 3 were used to derive the DSD moments, and from there, the parameters N_w and D_m using well-established formulas e.g. [28] and [26]. They are shown as '+' points in Fig. 4 and marked with the Figure number corresponding to the four events. The red dashed line represents the stratiform-convective rain separation line from the previous studies ([14], [15], [16]). The points for Fig. 2a and 3a lie below the separation line, hence categorized as stratiform rain, and those for Fig. 2c and 3c lie above the separation line, thus categorized as convective rain. These are indeed consistent with the radar observations for all four events.

Also in our previous studies, a simple 'index' parameter, i, (empirically-derived) was used to indicate whether the N_w versus D_m lie above or below the separation line. Stratiform rain is indicated by i when it is negative and convective rain is indicated by i when it is positive. The same procedure is used here. The index values (derived from 3-minute DSD based $N_w – D_m$) for the 14 October 2019 are shown in Figure 5 for the whole duration of the event. The separation line (i.e. i=0) is also included. As seen, there are several cases with positive i or i close to 0. These are numbered from (i) through to (vii).The corresponding RHI scans from NPOL are given in Fig. 6. In all cases, the arrows point to the precipitation structure above the disdrometers.
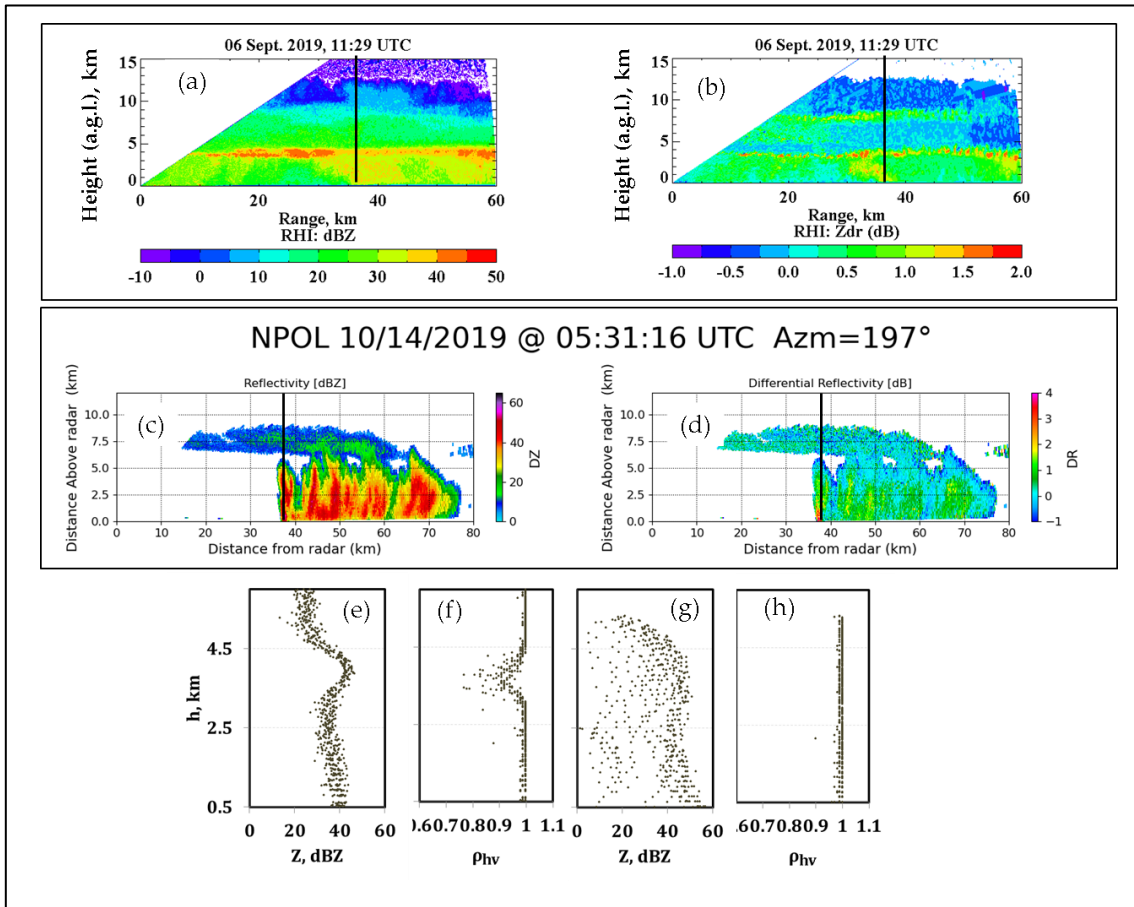
Figure 3. (a) RHI scan of Z_h and **(b)** Z_{dr} during a stratiform rain event on 6 September 2019 (Rain-bands of Dorian storm); **(c)** and **(d)** RHI scans of Z_h and Z_{dr} during another convective rain event on 14 October 2019; **(e)** and **(f)** vertical profiles of Z_h and ρ_{hv} respectively over the disdrometers for case (a); **(g)** and **(h)** vertical profiles of Z_h and ρ_{hv} respectively over the disdrometers for case (c).
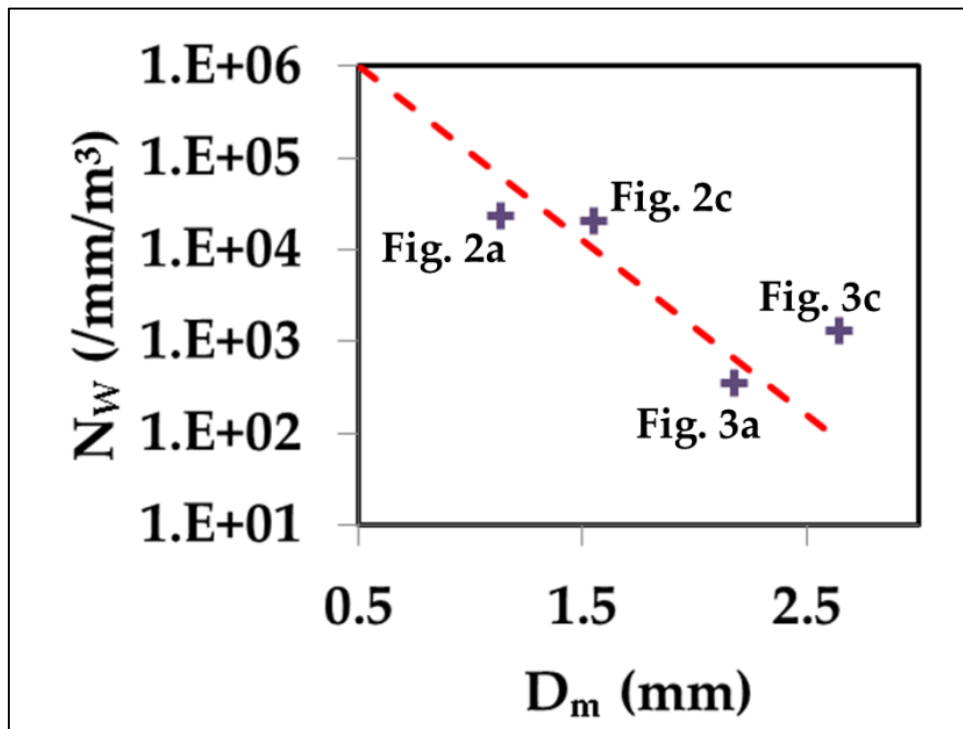
Figure 4. N_W versus D_m from 1 or 3 minute DSDs corresponding to Fig. 2(a), 2(c), 3(a), and 3(d), as marked.
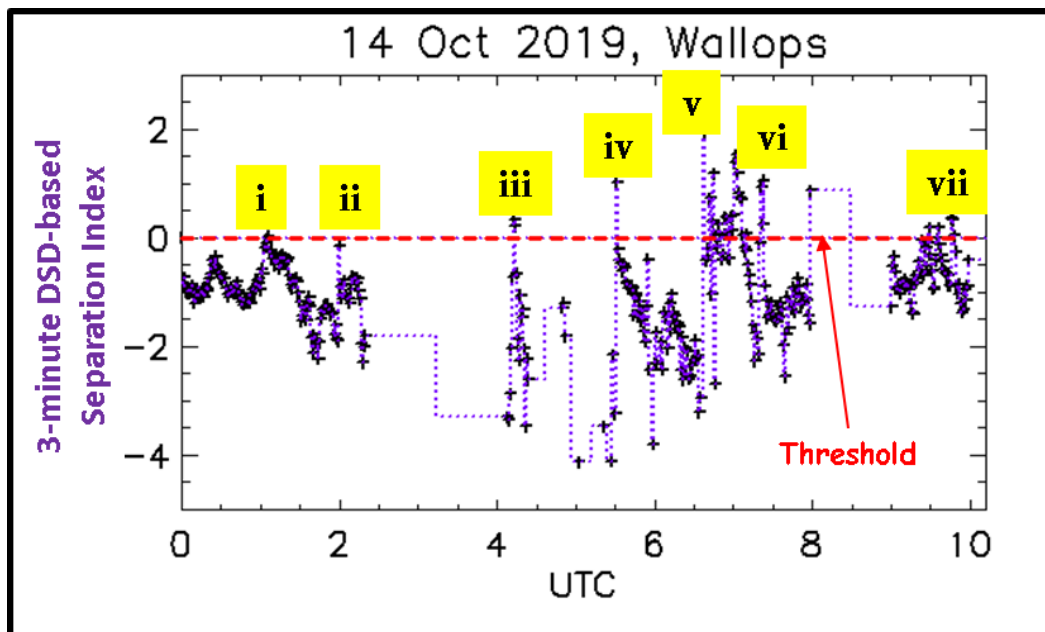

Figure 5. Variation of the 'index' parameter with time for the 14 October 2019 event. Cases (i) to (vii) are marked where the index reaches close to or above 0 threshold.

Cases (i) and (ii) have relatively thick bright-bands, and from Fig. 5 we see that the index values approach zero. By comparison, in [16], DSD and profiler data during a 'cold-rain' event in Ontario, Canada, showed that the index i became closer to zero with bright-band peak values within the melting layer in stratiform rain. Given that thicker bright bands have higher dBZ peaks, cases (i) and (ii) in Fig. 6 appear to be consistent with the results from the Ontario event.

Case (iii) from Fig. 6 shows convective rain over the disdrometer site but relatively moderate in intensity and is limited in its size, that is, its core spans less than 5 km in range. For this case, the index lies just above the red line.

Cases (iv), (v) and (vi) are more typical of convective rain, but the strong echoes, unlike deep convection, do not reach very high heights. Nevertheless, the index values are significantly above the zero threshold.

Case (vii) can be categorized as shallow convection (from last panel of Fig. 6), with echo tops being below 5 km a.g.l. For this case, the index lies just above zero. D_m values during this period were lower than those during cases (iv), (v) and (vi) (not shown here).

Next, we consider the event on 16 October 2019. This too lasted for several hours, and the index values based on 3-minute DSDs are shown in Fig. 7. They go above the zero threshold only at around 17:00 UTC. Three time periods are marked: (i) which is well below zero, (ii) which is a little above zero, and (iii) which is negative but close to zero.

The corresponding NPOL RHI scans ae given in Fig. 8. Case (i) does not show a clear bright-band in dBZ but the Z_{dr} plot shows the enhancement more clearly. The RHI scan from case (ii) appears to indicate modest convection over the disdrometer site, although the Z_{dr} plot shows enhancement beyond 40 km range. One could classify this case as 'mixed' or 'transition'. Case (iii) is a thick bright-band case, with high dBZ peak in the melting layer (> 50 dBZ). The index value at this time is very similar to case (i) of the 14 October event shown earlier in Fig. 5 and Fig. 6.
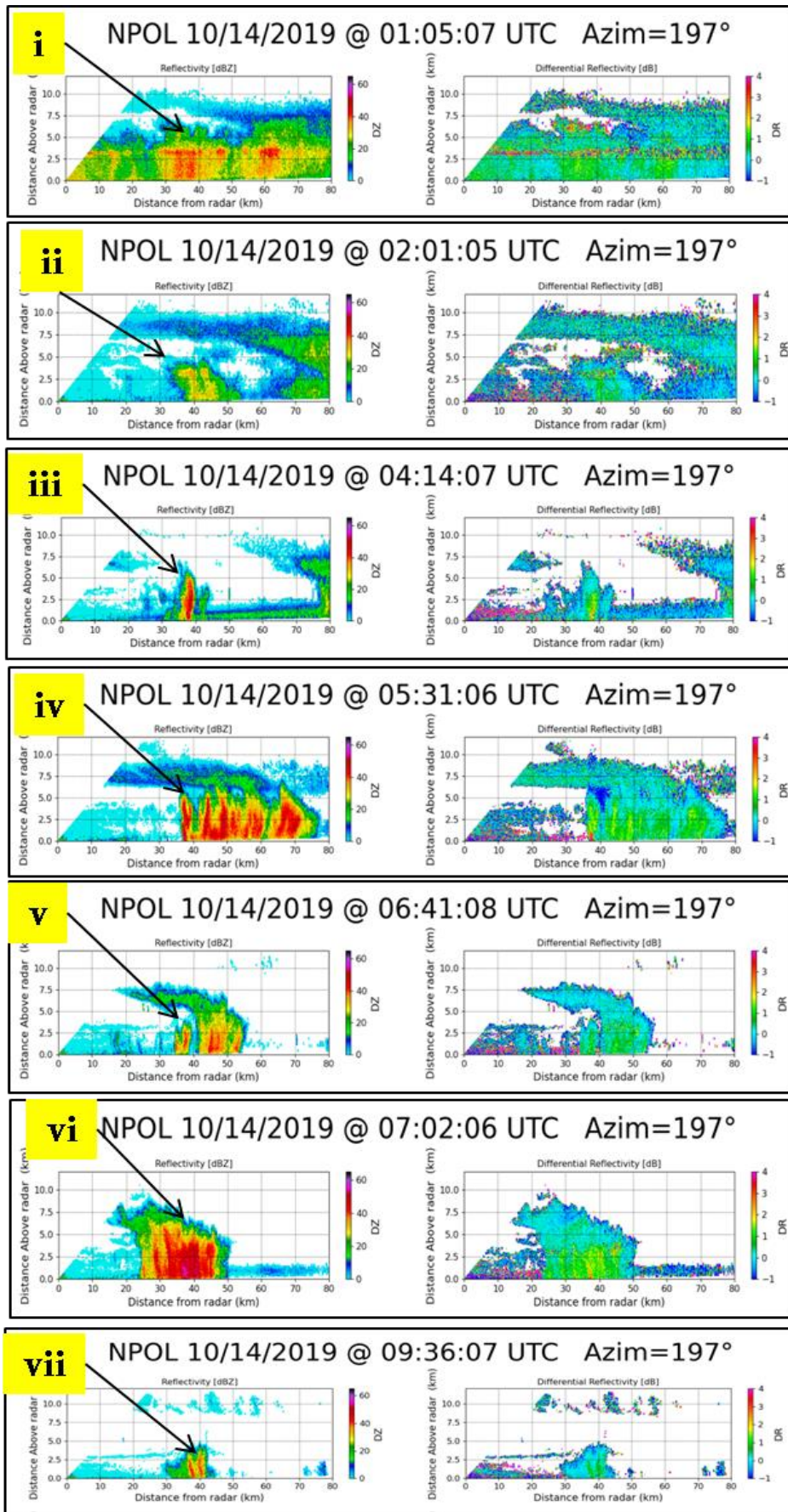
Figure 6. NPOL RHI scans of Z_h and Z_{dr} corresponding to cases (i) to (vii) in Figure 5.
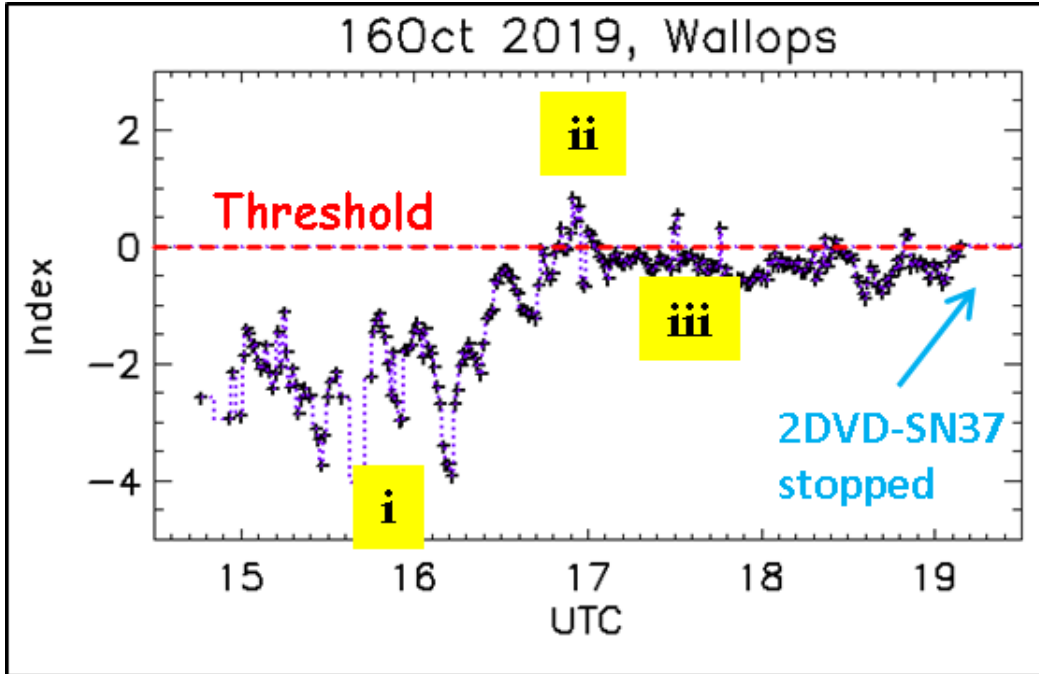

Figure 7. Variation of the 'index' parameter with time for the 16 October 2019 event. Cases (i), (ii) and (iii) are marked where the index indicated stratiform, convective and 'mixed' or 'uncertain' rain, respectively.
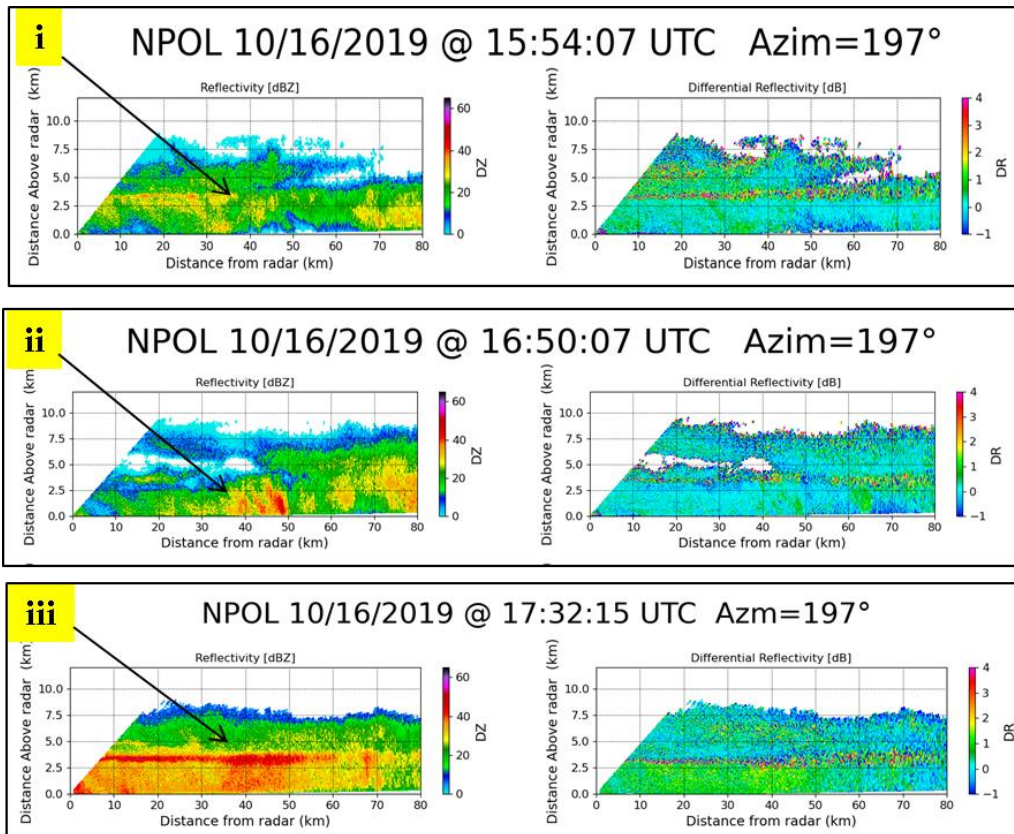
Figure 8. NPOL RHI scans of Z_h and Z_{dr} corresponding to cases (i), (ii) and (iii) in Fig. 7.

4. Rain-bands of Hurricane Dorian

This event also lasted for many hours over the Wallops site. The N_W and D_m from the measured 3-minute DSDs from are shown in Figure 9(a) and (b), and their variation against one another is shown in panel (c) where the colors represent different hours (as shown in the figure). Also shown is the separation line as dashed black line.

According to the DSD-based classification much of this event was stratiform rain. This is in agreement with the regular NPOL RHI scans taken throughout the event (not shown here). There is however a few points that appear to lie above the black line in panel (c). They are mostly in the 15 to 16 h UTC and have $D_m > 2$ mm. From panel (b), we see that the points correspond to 15:30 to 16:00 UTC. The index values are shown panel (d) where slightly positive values can be seen.
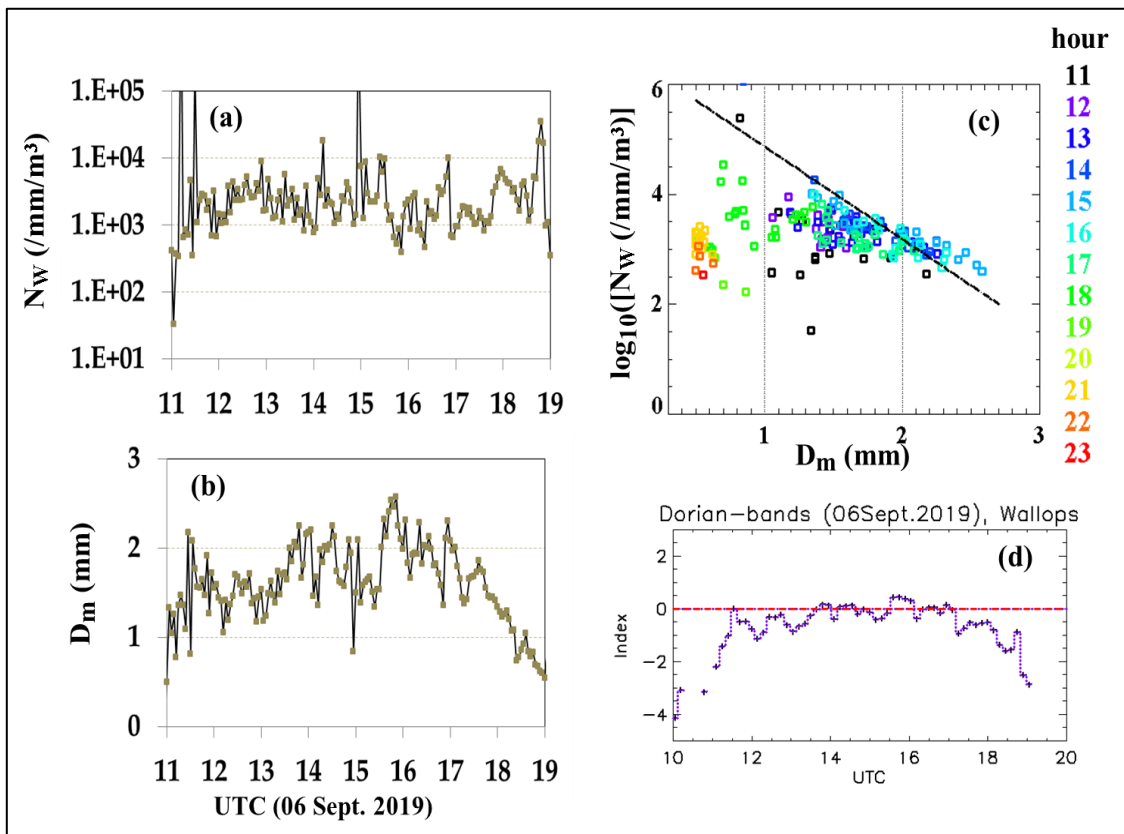
Figure 9. (a) N_W and **(b)** D_m variation with time from the 3-minute composite DSDs; **(c)** $\log_{10}(N_w)$ versus D_m rom the 3-minute DSDs for each hour (color-coded).

During this time period, several large drops were recorded by the 2DVD, including a very large (fully melted) drop with D_{eq} of 8 mm. An RHI scan at 15:41 UTC is shown in panels (a) and (b) of Fig. 10. The rain type is very definitely stratiform rain with clearly defined bright-band both in Z_h and Z_{dr}. Panels (c) and (d) show the vertical profiles of Z_h and ρ_{hv} over and surrounding the disdrometers. Similar to Fig. 3(e) and 3(f), Z_h profiles show very clear peak (4 to 4.5 km for this case) and the ρ_{hv} profiles show a corresponding dip in the melting layer. Hence for this case, i.e. between 15:30 and 16:00 UTC, our DSD-based classification did not correctly identify the rain type. One feature worth noting in the RHI scan is the layer of enhanced Z_{dr} at around 8 km height. This has been attributed to dendritic growth zone which typically occurs at around -15 deg C height [30].

5. Summary

Over a total of 20 hours of DSD data from three events in the Delmarva peninsula have been tested. The DSD-based classification correctly identified stratiform and convective rain types for all cases throughout all three events except for a 30-minute period during the event relating to Hurricane Dorian rain-bands. This 30-minute period was unusual in that there were many large drops, including one with a D_{eq} of 8 mm (fully melted) drop, and yet a clear bright-band was present around the 0 degree C isotherm height. However, the bright-band thickness and the dBZ peak were high.

Data and observations from two other locations, i.e. Huntsville, Alabama, and Greeley, Colorado (as well as Ontario, Canada) have supported the separation line in the $N_W - D_m$ space. Additionally, in Figure 11 we show the separation line along with some readily available data points from [5]. Based on the location and rain-types (either from radar observations or using the standard deviation of rain rate with time), these data points were classified into (i) stratiform rain, (ii) tropical-convective, and (iii) continental-convective rain. Their locations, and the mean values of D_m and $\log_{10}(N_W)$, together with the corresponding standard deviations are presented in Table 1. They are from different continents and have very different climatologies, but even so, our $N_W - D_m$ line seem to separate the stratiform and convective rain types for all cases.

Finally, in Appendix A, we demonstrate how the $N_W - D_m$ separation technique can be used to identify convective and stratiform rain regions from NPOL radar scans.
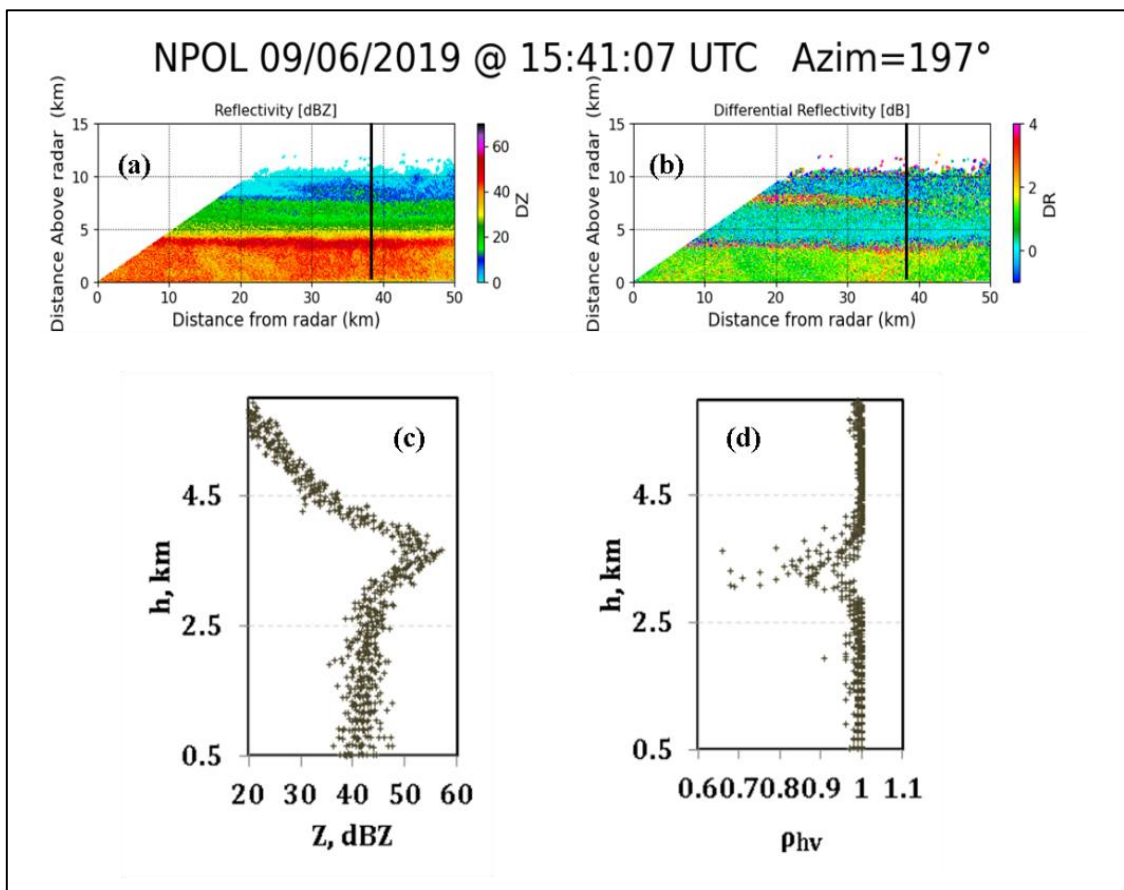

Figure 10. (a) RHI scan of Z_h; **(b)** Z_{dr} during a stratiform rain event (with thick bright-band) on 6 September 2019, i.e. rain-bands of Dorian storm; **(c)** and **(d)** vertical profiles of Z_h and ρ_{hv} respectively over the disdrometers (black lines in panel (a) and (b)).
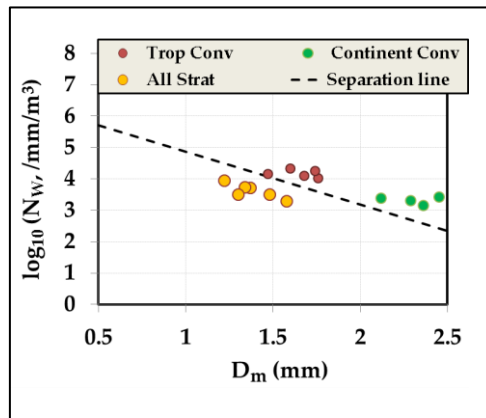
Figure 11. $\log_{10}(N_w)$ versus D_m for some locations and rain-types from [5], as given in Table 1.

Table 1. Locations and disdrometer types for data points used in Fig. 11, along with the mean values of D_m and $\log_{10}(N_w)$, and their corresponding standard deviations.

	Site (Disdrometer type)	$<D_m>$ mm	Std dev. of D_m in mm	Log $<N_w>$	Std dev. of log N_w
Tropical Conv	Darwin (Joss)	1.68	0.385	4.1	0.36
	SCSMX (Joss)	1.76	0.326	4.03	0.312
	Papua New Guinea (2DVD)	1.47	0.32	4.15	0.327
	Florida (2DVD)	1.74	0.49	4.25	0.52
	TOGA-COARE (from airborne data)	1.6	0.34	4.33	0.4
Continent Conv	Graz (2DVD)	2.12	0.53	3.39	0.45
	Sydney(Joss)	2.29	0.51	3.3	0.34
	Arecibo (Joss)	2.36	0.17	3.15	0.27
	Colorado (2DVD)	2.45	0.58	3.43	0.38
All Strat	Darwin (Joss)	1.37	0.31	3.72	0.4
	SCSMX (Joss)	1.34	0.28	3.73	0.35
	Papua New Guinea (2DVD)	1.22	0.31	3.94	0.52
	Florida (2DVD)	1.48	0.34	3.5	0.48
	TOGA-COARE (from airborne data from Testud)	1.3	0.28	3.49	0.5
	Colorado(2DVD)	1.58	0.3	3.28	0.24

(JOSS: Joss Waldvogel disdrometer; SCSMX: South China Sea Monsoon Experiment; TOGA-COARE: Tropical Ocean-Global Atmosphere – Coupled Ocean Atmosphere Response Experiment).

Appendix A

The DSD based separation technique can also be used to identify stratiform and convective rain regions from NPOL radar scans. It entails, as a first step, the estimation of the two DSD parameters needed for the separation, N_W and D_m. Initially, the mass-weighted mean diameter, D_m, is estimated using the S-band Z_{dr} via a two-step procedure which involves an intermediate parameter, D_m', as defined in [31]. D_m' depends on two (chosen) reference DSD moments. In [32], where X-band polarimertic radar retrievals were successfully carried out, the chosen reference moments were the 3rd and the 6th moments. We use a similar approach here, except the frequency is now S-band.

Scattering (T-matrix) calculations using 3-minute DSD spectra (from the Greeley and Huntsville campaigns) have been used to derive the retrieval equations. Fig. A1 shows the variations of (a) D_m' with the S-band Z_{dr}, (b) D_m with D_m', and (c) N_W/Z_h(linear) versus D_m'. The fitted equations are given in each of the panels. These were applied to the radar scans, and the results are shown in Fig. A2 for the two cases presented earlier in Fig. 2. Panels (a) to (d) correspond to the Dorian rain bands event on 06 Sept. 2019, at 11:29 UTC and panels (e) to (h) correspond to 14 October 2019 at 05:31 UTC. For both cases, the retrieved N_W and D_m are shown in panels (a),(e), (b) and (f) respectively, and the index values are shown in panels (c) and (g). Only the rain region is shown in all cases, up to 3 km above ground level. Note also for the second event, the radar range goes from 35 km to 60 km since there was no precipitation at closer range. The retrieved N_W versus D_m from the radar scans (below 3 km height) are shown in panels (d) and (h), with the separation line (in red) over-plotted.

The differences between the two events can be clearly observed from Fig. A2. N_W shows more uniformity for the stratiform rain event and D_m shows higher values for some regions in the convective event. The index values are mostly negative for the 06 Sept. 2019 case and mostly positive for the 14 Oct. 2019 case. This not only lends support to the separation method (largely) but also provides general support to our retrieval method for the DSD parameters from the NPOL radar scans. Note also from panels (d) and (h) that most points lie below the red line for the stratiform rain case, except for very low D_m points (which need to categorized as light rain event and considered separately) , while most points lie above the red line for the convective rain case.
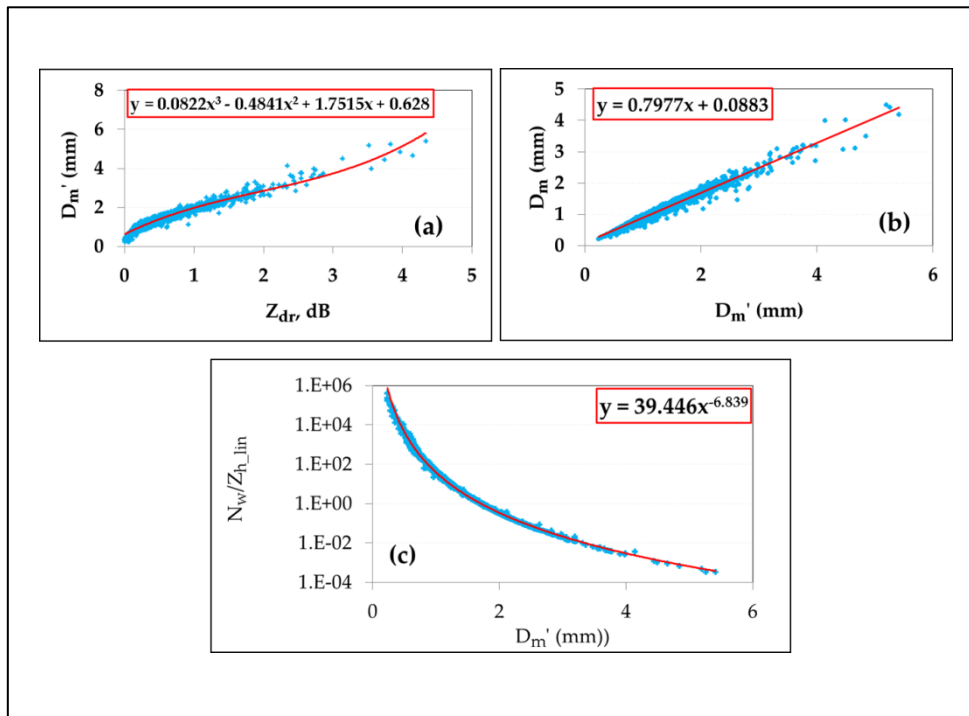

Figure A1. S-band simulation results of **(a)** D_m' versus Z_{dr}; **(b)** D_m with D_m'; **(c)** N_W/Z_h(*linear*) versus D_m'.
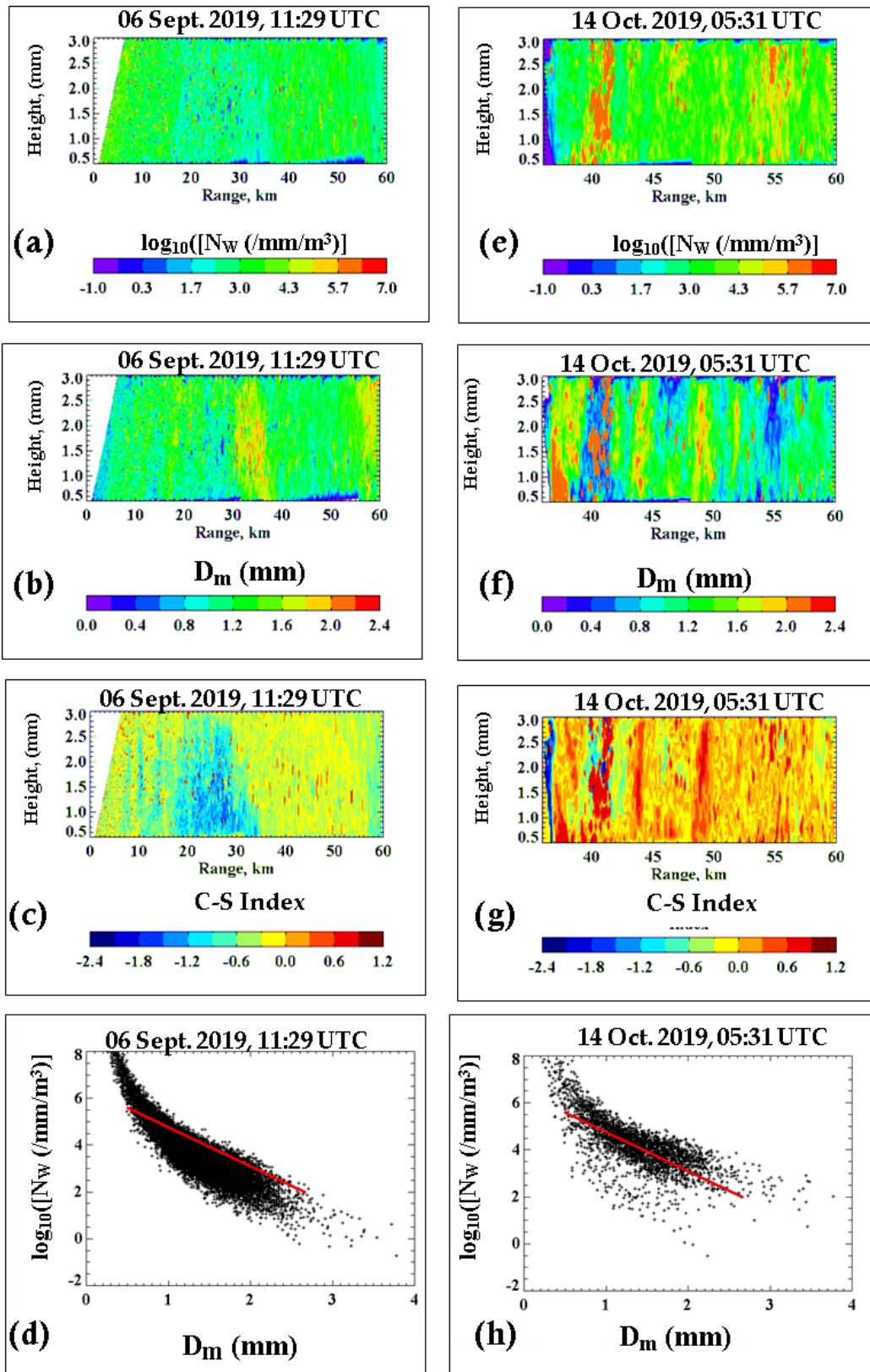
Figure A2. Retrievals from NPOL-RHI scans from the 06 Sept. 2019 event (left panels) and from the 14 Oct. 2019 event (right panels). **(a)**, and **(e)** show the retrieved N_W; **(b)** and **(f)** show the retrieved D_m; **(c)** and **(g)** show the index values and **(d)** and **(h)** show the N_W versus D_m for the two cases.

Author Contributions: Conceptualization, M.T. and V.N.B.; Methodology, Investigation and Formal Analysis, M.T. and V.N.B.; Data Curation, D.M., D.B.W. and C.P.; Writing-Original Draft Preparation, M.T.; Writing-Review & Editing, V.N.B.; D.B.W.; Supervision, V.N.B.; Resources, D.B.W.

Conflicts of Interest: The authors declare no conflict of interest. The funders had no role in the design of this study; in the collection, analyses, or interpretation of its data; in the writing of this manuscript, and in the decision to publish these results.

References

1. Steiner, M.; Houze, R.A.; and Yuter, S. E. Climatological Characterization of Three-Dimensional Storm Structure from Operational Radar and Rain Gauge Data. *J. Appl. Meteor.*, **1995**, *34*, 1978–2007.
2. Tao, W.; Iguchi, T.; Lang, S. Expanding the Goddard CSH Algorithm for GPM: New Extratropical Retrievals. *J. Appl. Meteor. Climatol.*, **2019**, *58*, 921–946.
3. Houze, R. A., Jr. Cloud Dynamics. Academic Press, **1993**, 573 pp.
4. Tokay, A.; Short, D. A. Evidence from Tropical Raindrop Spectra of the Origin of Rain from Stratiform versus Convective Clouds. *J. Appl. Meteor.*, **1996**, *35*, 355–371,
5. Bringi, V.N.; Chandrasekar, V.; Hubbert, J.; Gorgucci, E.; Randeu, W.L.; Schoenhuber, M. Raindrop Size Distribution in Different Climatic Regimes from Disdrometer and Dual-Polarized Radar Analysis. **2003**, *J. Atmos. Sci.*, *60*, 354–365.
6. Thompson, E. J.; Rutledge, S. A.; Dolan, B.; Thurai, M. Drop Size Distributions and Radar Observations of Convective and Stratiform Rain over the Equatorial Indian and West Pacific Oceans. *J. Atmos. Sci.*, **2015**, *72*, 4091–4125.
7. Atlas, D.; Ulbrich, C. W.; Marks Jr., F. D.; Black, R. A.; Amitai, E.; Willis, P. T.; Samsur, C. E. Partitioning tropical oceanic convective and stratiform rains by draft strength. *J. Geophys. Res.*, **2000**, *105*, 2259–2267.
8. Testud, J.; Oury, S.; Black, R.A.; Amayenc, P.; Dou, X. The concept of "normalized" distribution to describe raindrop spectra: A tool for cloud physics and cloud remote sensing. *J. Appl. Meteorol.* **2001**, *40*, 1118-1140.
9. Ulbrich, C. W.; Atlas, D. On the separation of tropical convective and stratiform rains. *J. Appl. Meteor.*, **2002**, *41*, 188–195.
10. Yuter, S. E.; Houze Jr., R. A. Measurements of raindrop size distributions over the Pacific warm pool and implications for Z–R relations. *J. Appl. Meteor.*, *1997*, *36*, 847–867.
11. Bukovcic, P.; Zrnic, D.; Zhang, G. Convective–stratiform separation using video disdrometer observations in central Oklahoma – the Bayesian approach. *Atmospheric Research*, **2009**, *155*, 176–191.
12. Schoenhuber, M.; Lammer, G.; Randeu, W. L. One decade of imaging precipitation measurement by 2D-video-distrometer. *Adv. Geosci.* **2007**, *10*, 85-90.
13. Schönhuber, M.; Lammer, G.; Randeu, W.L. The 2D-Video-Distrometer. In Precipitation: *Advances in Measurement, Estimation and Prediction; Michaelides*, S., Ed.; Springer: Berlin/Heidelberg, Germany, **2008**; pp. 3-31. ISBN 978-3-540-77654-3.
14. Bringi, V. N.; Williams, C. R.; Thurai, M.; May, P. T. Using dual-polarized radar and dual-frequency profiler for DSD characterization: A case study from Darwin, Australia. *J. Atmos. Oceanic Technol.*, **2009**, *26*, 2107–2122.
15. Thurai, M.; Bringi, V. N.; May, P. T. CPOL radar-derived drop size distribution statistics of stratiform and convective rain for two regimes in Darwin, Australia. *J. Atmos. Oceanic Technol.*, **2010**, *27*, 932–942.
16. Thurai, M.; Gatlin, P.N.; Bringi, V.N. Separating stratiform and convective rain types based on the drop size distribution characteristics using 2D video disdrometer data, *Atmospheric Research*, **2016**, *169, Part B*, 416-423.
17. Thurai, M.; Kennedy, P.; Dolan, B.; Bringi, V. N. Testing the DSD-Based Stratiform-Convective Rain Separation for Ten Events in Greeley, Colorado, *38th Conference on Radar Meteorology*, **2017**, *paper-poster 24*, Chicago, USA.

18. Knollenberg, R. The optical array: an alternative to scattering or extinction for airborne particle size determination, *J. Appl. Meteorol.* **1970**, *9*, 86–103.

19. Baumgardner, D.; Kok, G.; Dawson, W.; O'Connor, D.; Newton, R. A new ground-based precipitation spectrometer: The Meteorological Particle Sensor (MPS). *11th Conf. on Cloud Physics, Ogden, UT, Amer. Meteor. Soc.,* **2002**, *paper 8.6.*

20. Bringi, V.N.; Thurai, M.; Baumgardner, D. Raindrop fall velocities from an optical array probe and 2-D video disdrometer. *Atmos. Meas. Tech.* **2018**, *11*, 1377-1384.

21. Bringi, V. N.; Hoferer, R.; Brunkow, D. A. ; Schwerdtfeger, R.; Chandrasekar, V.; Rutledge, S. A.; George, J.; Kennedy, P. C. Design and Performance Characteristics of the New 8.5-m Dual-Offset Gregorian Antenna for the CSU–CHILL Radar. *J. Atmos. Oceanic Technol.,* **2011**, *28*, 907–920.

22. Skofronick-Jackson, G.; Petersen, W.A.; Berg, W.; Kidd, C.; Stocker, E.F.; Kirschbaum, D.B.; Kakar, R.; Braun, S.A.; Huffman, G.J.; Iguchi, T.; et al. The Global Precipitation Measurement (GPM) Mission for science and society. *Bull. Am. Meteorol. Soc.* **2016**, *98*, 1679-1696.

23. Tokay, A.; Bashor, P. G.; McDowell, V. L. Comparison of Rain Gauge Measurements in the Mid-Atlantic Region. *J. Hydrometeor.,* **2010**, *11*, 553–565,

24. OTT Hydromet GmbH. Operating instructions: OTT Pluvio2 precipitation gauge. *OTT Hydromet* **2010**, 60 pp. [Available online   at http://www.ott.com/en-us/products/download/operating-instructions-precipitation-gauge-ott-pluvio2/]

25. Rasmussen, R.; Baker, B.; Kochendorfer, J.; Meyers, T.; Landolt, S.; Fischer, A. P.; Black, J.; Thériault, J.M.; Kucera, P.; Gochis, D.; Smith, C.; Nitu, R.; Hall, M.; Ikeda, K.; Gutmann, E. How Well Are We Measuring Snow: The NOAA/FAA/NCAR Winter Precipitation Test Bed. *Bull. Amer. Meteor. Soc.* **2012**, *93*, 811–829.

26. Raupach, T.H.; Thurai, M.; Bringi, V. N.; Berne, A. Reconstructing the Drizzle Mode of the Raindrop Size Distribution Using Double-Moment Normalization. *J. Appl. Meteor.* **2019**, Climatol., *58*, 145–164.

27. Wolff, D.B., D.A. Marks, and W.A. Petersen, 2015: General Application of the Relative Calibration Adjustment (RCA) Technique for Monitoring and Correcting Radar Reflectivity Calibration. *J. Atmos. Oceanic Technol.,* **2015**, *32*, 496–506.

28. Thurai, M.; Bringi, V.N.; Wolff, D.B.; Marks, D.A.; Pabla, C.S. Drop Size Distribution Measurements in Outer Rainbands of Hurricane Dorian at the NASA Wallops Precipitation-Research Facility. *Atmosphere*, **2020**, *11*, 578.

29. Bringi, V.; Seifert, A.; Wu, W.; Thurai, M.; Huang, G.-J.; Siewert, C. Hurricane Dorian Outer Rain Band Observations and 1D Particle Model Simulations: A Case Study. *Atmosphere,* **2020**, *11*, 879.

30. Kennedy, P.C.; Rutledge, S.A. S-Band Dual-Polarization Radar Observations of Winter Storms. *J. Appl. Meteor. Climatol.* **2011**, *50*, 844–858.

31. Lee, G. Zawadzki, I., Szyrmer, W.; Sempere-Torres, D.; Uijlenhoet, R. A General Approach to Double-Moment Normalization of Drop Size Distributions. *J. Appl. Meteor.,* **2004**, *43*, 264–281.

32. Bringi, V.N.; Mishra, K.V.; Thurai, M.; Kennedy, P.C.; Raupach, T.H. Retrieval of lower-order moments of the drop size distribution using CSU-CHILL X-band polarimetric radar: a case study. *Atmos. Meas. Tech.,* **2020**, *13*, 4727–4750.